DOI 10.5162/sensoren2024/P10

Advanced Self-X Architecture for Improved Angle Accuracy Restoration in TMR-Based Angular Decoders

Elena Gerken[1], Qummar Zaman[1], Senan Alraho[1], and Andreas König[1]
[1] Cognitive Integrated Sensor Systems, University of Kaiserslautern-Landau, Deutschland, gerken@eit.uni-kl.de

Summary

This work delves into the vital role of self-X systems within sensor technology, underlining their increasing significance in boosting system robustness and reliability, and provides a concise list of possible sensor failures, illustrating the broad spectrum of challenges in sensory system lifetimes. The study begins by applying self-X principles inspired by biological immune system (BIS), particularly its inherent ability to autonomously detect and respond to anomalies. It specifically examines the implementation of self-X concepts in xMR-angular decoders, adopting a hierarchical approach to demonstrate their practical effectiveness in sensor systems. This research includes upgrades to the experimental setup, integrating autonomous offset calibration through digital offset auto zeroing in a self-X equipped reconfigurable analog front end (AFEX), along with a 4th-order active low pass filter for considerable noise reduction. The focus on offset and gain adjustments is presented as an initial step towards a more comprehensive work aimed at addressing a wide array of known sensor issues. A key finding of this study is the significant reduction of an initial angular decoding error from 6.337° to 0.462°, a 92.71% improvement, demonstrating the effectiveness of the advanced self-X architecture. This dynamic approach marks a significant shift from static methods, providing a strong foundation for future developments in the areas of sustainability and autonomy of sensor systems.

Keywords: Self-X System, Self-X-Hierarchy, TMR-Based Decoder, Self-Monitoring, Self-Healing.

Introduction

The landscape of sensor technology, especially in measuring and control systems for Industry 4.0, is transforming, with a shift towards enhancing efficiency, reducing human intervention, and elevating robustness and reliance [1,2]. Leading this major change is the new idea of self-X (self-healing, self-calibration, self-repairing, etc.) concept, which is a key step forward in the design of smart sensory systems [3-5].

Inspired by the autonomy of living beings, the self-X features is a comprehensive concept that encompasses a wide range of system self-managing functions [6]. The artificial immune system (AIS) algorithms play a vital role in supporting measurement system with self-X properties [7, 8]. It is responsible for significantly enhancing the system's autonomous fault detection and repair capabilities, reflecting the self-managing properties inherent in biological immune BIS [9]. This integration leads to the development of sensory systems that are not only more reliable and resilient but also highly adaptive, meeting the evolving demands of Industry 4.0 [10]. AIS mechanisms enable systems to not only adapt to changing operational conditions but also dynamically respond to environmental changes and potential malfunctions. This ensures the continuity and reliability of processes in various conditions [9].

In this paper, we explore the advanced self-X architecture application in tunnel magnetoresistance (TMR) based angular decoders, focusing on its ability to recover and maintain relative quality performance amidst perturbations and defects. The experimental setup involves a TMR sensor responding to a magnetic field from a permanent magnet. The field changes with the magnet's angle to the sensor, altering the sensor materials' resistance [11]. The TMR sensor detects changes in resistance caused by the angle between the magnetic field and its elements. This change is converted into electrical signals to calculate the magnet's angle relative to the sensor. Two elements positioned at 90 degrees measure the magnetic field's sine and cosine, with arctangent calculations providing precise angles [11]. The accuracy of TMR sensor measurements can be affected by various types

of errors [12-14]. In the left part of Figure 1, the ideal positioning of TMR sensor relative to the magnet is shown. In the right part of the figure, possible mechanical errors leading to inaccuracies in angular measurements due to changes in the magnetic field are depicted. These errors can include incorrect alignment or eccentricity of the magnet, as well as improper positioning or tilting of the sensor.

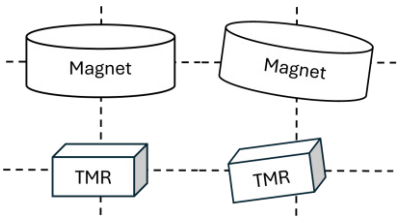

Fig. 1: Sources of TMR sensor mechanical errors.

Measurement errors related to non-linearity occur when the sensor's output signal does not change proportionally to the input magnetic field and include amplitude mismatch, signal offset, phase errors, and signal distortions [12], as shown in Figure 2.

Signal chain errors, arising from limitations in the sensor's electronic circuitry, include arbitrary (increasing) number of tunnel junctions, imperfect magnetization of system magnet, mismatch in sensitivity between channels, input offset, noise, quantization errors, signal propagation delays, and the influence of temperature changes [12]. In ideal conditions, when using a TMR sensor for angular measurements, the output signals of sine and cosine should form a perfect circle centered at point (0,0) on the graph. However, due to various measurement errors, this curve can be significantly distorted [14]. These distortions and deviations are visually represented and analysed in Figure 3.

Amplitude mismatch between the sine and cosine signals can turn the circle into an ellipse, affecting the accuracy of angle determination. Signal offset relative to zero shifts the circle's center from point (0,0), which can also lead to inaccurate angular measurements [14]. Phase error, occurring if the phase relationship between sine and cosine differs from 90 degrees, deforms the curve shape. Furthermore, signal distortions, such as irregularities or noise, can cause roughness or "teeth" on the curve, reducing measurement accuracy.

The self-X architecture, grounded in a hierarchical approach, is constructed in both hardware and software layers.

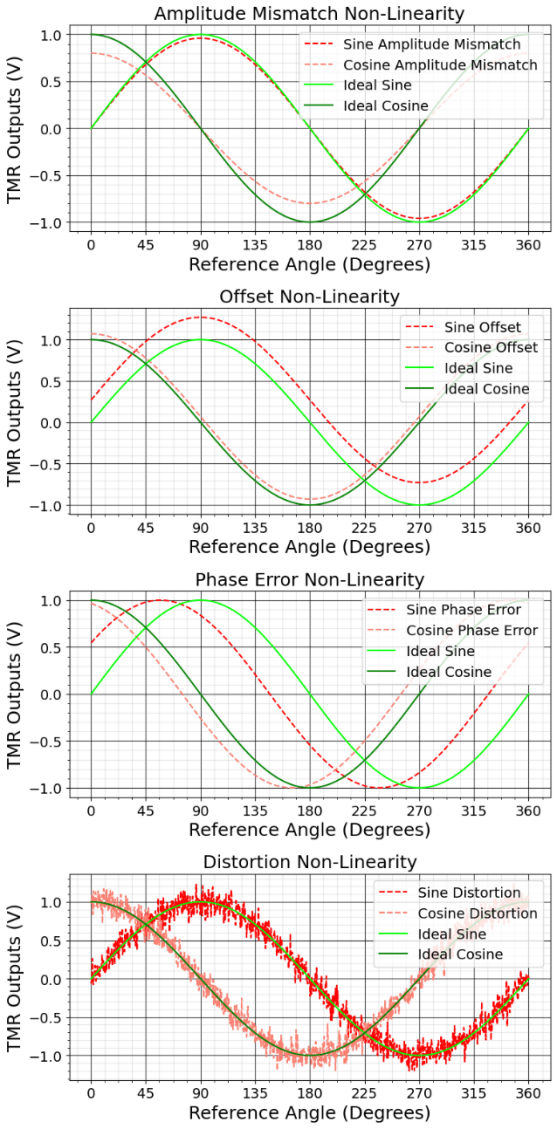

Fig. 2: Distorted TMR sensor signals.

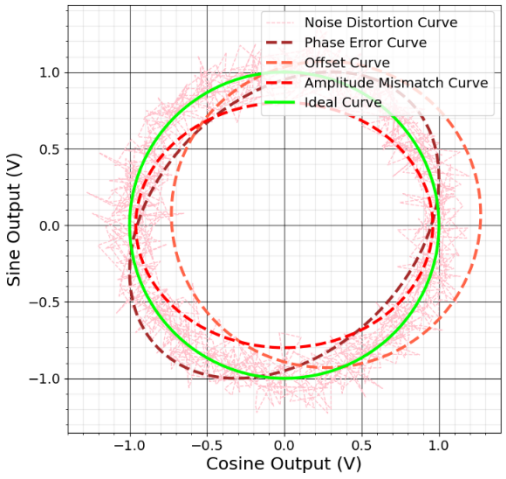

Fig. 3: Graphical representation of distorted TMR sensor Lissajous patterns.

The software layer, driven by AIS algorithms, is dedicated to complex tasks such as system monitoring and anomaly detection, utilizing data from TMR sensors. Concurrently, the hardware layer specializes in online fault correction, integrating self-healing properties for real-time response and effective recovery. This well-defined division of roles within the self-X-hierarchy, where software is responsible for detection and hardware for correction, ensures dynamic adaptability and robust system performance. It greatly enhances the capabilities of intelligent systems to efficiently handle and adapt to a variety of operational challenges.

The main goal of this work is to explore the practical implementation of the self-X-hierarchy in the TMR measurement system, particularly focusing on its reliability and fault tolerance, especially in addressing challenges posed by mechanical faults.

Proposed Methodology

Figure 4 depicts the flow diagram of the proposed TMR-based sensor measurement system, with self-X-hierarchy.

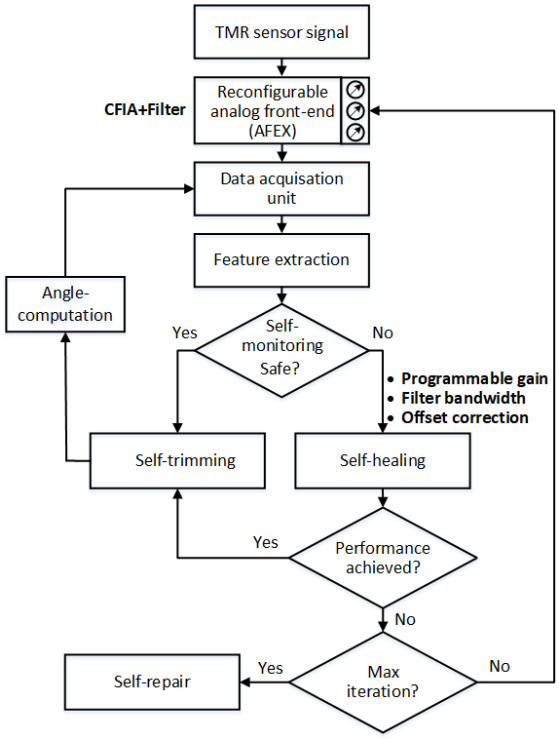

Fig. 4: The self-X-hierarchy for TMR measurement system.

The system, at its lowest hierarchical layer, consists of a reconfigurable analog front end with self-X features (AFEX), which integrate of a reconfigurable and programmable gain fully differential indirect current-feedback instrumentation amplifier (CFIA) followed by tuneable active CMOS-C fourth-order low pass filter [15, 16].

The data acquisition unit executes in real-time measurements the conditioned analog signal. It is powered by a field programmable gate array (FPGA) board, sourced from Red Pitaya. The sensor signal is precisely recorded using onboard low-noise, high-speed analog-to-digital converters (ADCs). The software hierarchical level involves the feature extraction unit, where features are calculated from the sine and cosine waves received from the TMR sensor. Subsequently, a feature selection process is implemented to eliminate correlations among the features. This is followed by dimension reduction. Next, the system engages in data self-monitoring, employing the refined features to diagnose system's operational state.

Self-monitoring mechanism operates by utilizing one-class classification. It compares incoming sensor data against a predefined 'normal' behaviour model, effectively determining if a signal matches normal operating parameters. This approach is inspired by BIS, mirroring its method of distinguishing between self and non-self-cells in living organisms. It's particularly suited to scenarios like fault monitoring in machinery, where normal operation data is available, and anomalies are seen as patterns not included in the training dataset. A positive selection algorithm (PSA), derived from BIS principles, and adapted in AIS algorithms is being utilized. The proposed algorithm, which combines NOVAS filtering method with PSA [17], requires only normal operational state samples during the training phase, significantly simplifying the error characterization process. A major advantage of PSA and NOVAS combination is its ability to detect anomalies without needing extensive historical data on system failures, which are often rare and hard to gather [18]. When the signal classification is deemed safe, the angular computation of the DC rotary motor is performed using the formula given below:

$$\theta = arctan\left(\frac{2A_{sin}\sin(\alpha+\varphi)+offset_{sin}}{2A_{cos}\cos(\alpha+\varphi)+offset_{cos}}\right) \quad (1)$$

Here, θ is the measured angle, α is the magnet rotational angle relative to the sensor, $2\mathcal{A}_{sin}$ and $2\mathcal{A}_{cos}$ are the peak sine and cosine amplitudes respectively, ϕ is the phase error between the sin and cos signal [19].

However, when the safe signal classification is false, the self-healing feature comes into play, which includes noise suppression, automatic offset calibration, and gain adjustment. This enables autonomous calibration of the sensory electronic system to adjust the circuit parameters to compensate for sensor signal

imperfections or faults caused by factors such as mechanical misalignments between the sensor and magnet.
Self-trimming is implemented in the software layer, based on ellipse fitting, which is used to simulate and tune sensor outputs, improving the accuracy of angle measurements by eliminating nonlinearities and inaccuracies in sensor readings. Self-repairing block indicating replacement of the TMR sensor if the self-healing process does not resolve the fault due to the self-X properties.

Experimental Setup

In this study, the Sensitec TFF953 TMR sensor is utilized. The laboratory setup is illustrated in Figure 5. Powered by a 3.3 V DC supply, this sensor comprises two balanced, fully-differential bridges, generating a pair of differential signals with a 90° phase shift (sine and cosine) and a central common mode voltage of 1.65 V. Signal processing is achieved using two FPGA Red Pitaya boards [19], leveraging their 14-bit ADCs each handling the sensor's amplified and filtered outputs via two AFEX chips [16]. A third FPGA board is exclusively used for AFEX chip configuration.

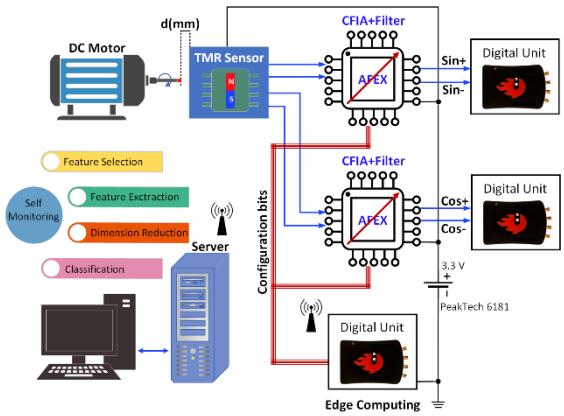

Fig. 5: The functional setup of the proposed interface with TMR sensor.

Although it's possible to use just two FPGAs for both signal processing and system configuration, by aligning their ground to the bridge's common mode voltage and the AFEX to 0 V, an alternative involves a DC level shifter for using only two FPGA boards. The server system manages the self-X algorithm for determining angles and detecting anomalies. The TMR sensor, attached to the DC motor's front rotary shaft, is also supplied by Sensitec.
Figure 6 outlines the TMR sensor readout circuit. The in-amp's digital offset voltage autozeroing capability [16, 20] is used for self-correcting the bridge's offset voltage, as implemented in [21]. This approach involves aligning the CFIA's reference point not to a fixed DC common mode voltage, typically half of the CFIA's supply range, but to the bridge's common mode voltage determined when the motor is idle. Other possibilities involve the use of chopper-type amplifiers, explored in [21,22], or adopting capacitive coupling methods, as in [23].

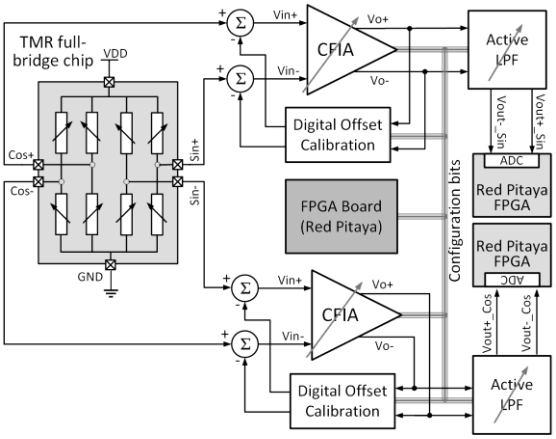

Fig. 6: The schematic diagram of the proposed TMR readout circuit.

The lab setup is depicted in Figure 7, demonstrating the complete TMR sensor interface.

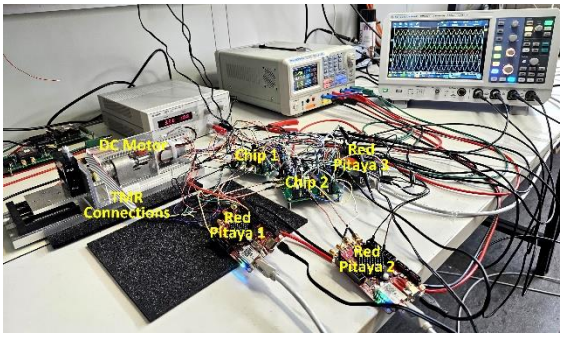

Fig. 7: Lab setup for TMR interface using the proposed AFEX chip.

Measurement Setup and Experimental Result

At the beginning, the filter cutoff frequency is set at 1 kHz, a more than tenfold higher than the rotational frequency of the demonstrator motor at for the performed experiment. This configuration ensures that there is no signal attenuation in the TMR outputs while with its fourth-order roll-off properties, still effectively attenuating the aliasing noise below the half of sampling frequency of the ADCs, running at 24.4 kS/s. The in-amp gain is initially set to unity to observe the TMR signal without amplification. The in-amp and the filter are configured by using the patterns found from the intrinsic optimization. The in-amp's gain is initially

adjusted to one, allowing for the observation of the TMR signal in its unamplified state. Configuration of the in-amp and the filter is guided by patterns identified through intrinsic optimization. To highlight the effect of offset voltage, the distance to the TMR sensor is set to 11 mm, requiring the gain to be increased to 32 to fit the full-scale voltage of the ADC. However, this adjustment reveals an output offset voltage close to 250 mV in corresponds to 7.812 mV of input offset voltage. The input offset voltage is a combination of the CFIA inherent offset voltage and the offset of the sensor bridge. Following the implementation of the autozeroing feature, the output offset voltage is successfully decreased to approximately 16 mV, in corresponds to 0.5 mV of input offset voltage as depicted in Figure 8.

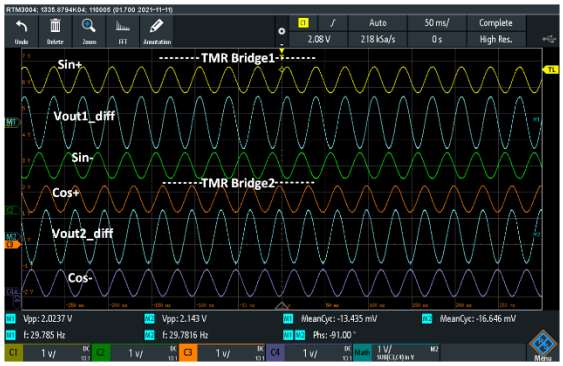

Fig. 8: TMR sensor outputs at the in-amp gain of 32, distance of 11 mm, filter bandwidth of 1 kHz and after applying the offset autozeroing.

The impact of the offset voltage extends beyond merely reducing the reading resolution by using up the ADC's full-scale voltage capacity. More importantly, it significantly affects the accuracy of angle computation, as specified in the equation detailed in [17].

System malfunctions were mechanically induced by altering displacement/eccentricity prior to data acquisition.

This was crucial for simulating real-world faults and testing the system's response capabilities.

From the training dataset, indicative of a normal state of system operation, features were extracted and categorized into time and frequency domains, with 24 and 22 features, respectively. In the time domain, dynamic characteristics of sampled signals were investigated, whereas in the frequency domain, the frequency spectrum of the incoming signal was used to derive features using Fast Fourier Transform. This approach, considering both time and frequency domains, ensures a thorough understanding of the signal's behaviour. Following feature selection, the most informative features displaying minimal correlation were chosen. These selected features were projected onto a two-dimensional space using nonlinear mapping (NLM). NLM is a technique aimed at reducing dimensionality while maintaining critical information. This process of projection resulted in the creation of a "safe zone", depicted by detectors of a normal system state on the 2-dimension plane. During the training phase, a collection of detectors illustrated in Figure 9 with varying radii ranging from 0.0065 to 0.0165 was established.

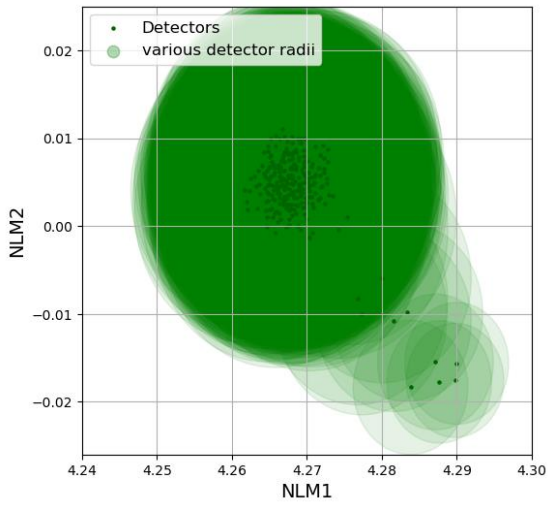

Fig. 9: Normal system operation state detectors.

The radii of detectors, forming the "safe zone", vary depending on the density of surrounding detectors. This design allows for a flexible and adaptive detection mechanism, capable of accurately identifying normal operating conditions and distinguishing them from potential anomalies or malfunctions.

The self-monitoring and self-healing process worked as follows: TMR testing data was gathered in real-time by the Red Pitaya measuring platform and sent to self-monitoring software layer located on a PC connected to a server. This data, in decimal coded .txt format, covered more than 1,000,000 samples, including over 4,000 samples per period. The motor speed of the experimental setup was set at 1413.63 rpm, and the sampling rate of Red Pitaya's ADC was 24.4 kHz. Self-monitoring converted the signal into voltage, selected and computed features, and then mapped them using NLM. Next, measured the distance from each new data point to the nearest detector. If the distance was within the detector's radius, the point was classified as part of the normal operational state of the TMR system and monitoring continued. However, if it exceeded the radius, the system flagged a potential

malfunction and automatically initiated a self-healing mechanism. During self-healing at the software layer, the optimal gain was computed and relayed to a programmable amplifier. At the hardware layer, signal filtering and offset adjustment occurred. Figure 10 illustrates the detector area characterizing the system's normal operational state, with signals identified as dangerous due to a sensor shift relative to the magnet from 4 to 11 mm, restored signal, facilitated by the self-healing mechanism is depicted in Figure 11.

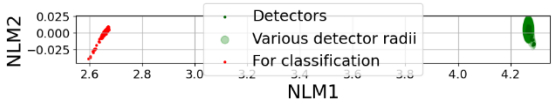

Fig. 10: Sensor position analysis and visualization of shift impacts from 4 to 11 mm.

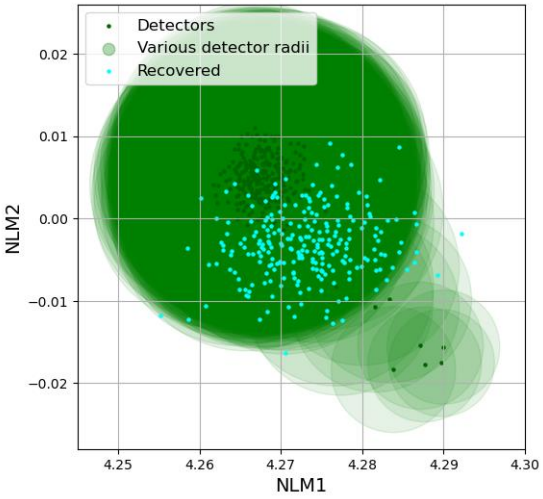

Fig. 11: Signal restoration after shift impacts from 4 to 11 mm.

With the noise supression and gain set at 4, Figure 12 displays a maximum absolute error of 6.337° at distance 11mm. To highlight the self-healing property, the experiment is repeated by subtracting noise, adjusting the gain to 32, eliminating offset, and addressing non-linearities using the ellipse fitting approach. The Lissajous curve, depicted in Figure 13, constructed from two sinusoidal signals at the sensor outputs, should ideally form a circle centered at (0,0) [14]. However, as shown in Figure 13, this is not the case with real sensor outputs. Thus, by employing software-based ellipse fitting to the Lissajous curve after the hardware-level recovery of TMR data, nonlinear components of the signal can be removed, thereby achieving a smaller angle calculation error. As a result, the application of the self-healing mechanism on both layers led to a significant reduction in the maximum angular error, reaching 0.462°, as shown in Figure 12.

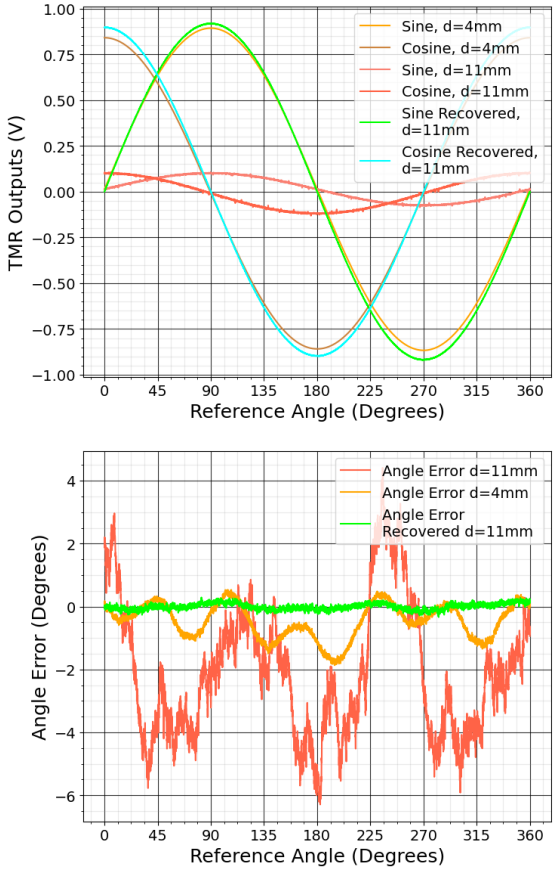

Fig. 12: TMR sensor angle computing error.

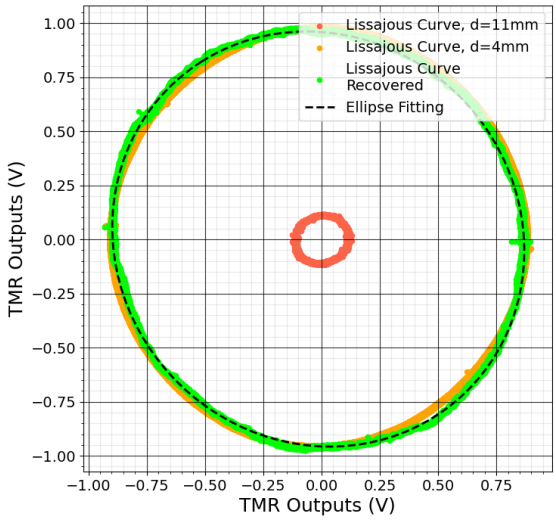

Fig. 13: Self-trimming using ellipse fitting.

Conclusion

This study demonstrates the significant advances possible in the field of sensor technologies, especially in the context of xMR angle decoders, through the introduction of self-

X systems inspired by the resilience and adaptability of biological immune systems.
Experimental results, such as a reduction in the decoding angle error after a perturbation from 6.337° to 0.462°, highlight the effectiveness of the self-X architecture. The 92.71% performance improvement is not only a testament to the system's accuracy, but also highlights the potential for wider application in a variety of sensor systems. The integration of self-healing capabilities such as noise suppression, automatic offset calibration, and gain control illustrates the system's ability to autonomously correct and adapt to changes and potential faults. The results of this study underscore the ability of the proposed self-X approach to restore and maintain relative performance in the face of mechanical impacts and defects. Such stability once again demonstrates the practical viability of the system under intricate operating conditions, opening new horizons for the application of self-X systems in complex and demanding environments.
Future work will focus on using multisensory input from a small set of redundant TMR sensors with both “soft” and “hard” defects. This approach involves introducing errors at the sensor level and exploring combinations of multiple sensors to improve overall system performance.

References

[1] Kadne, A., Kamath, P., Karvat, M., Bodkhe, M., Sharma, S. (2024). A Comprehensive Study on Industry 4.0 Technologies. In: Bhardwaj, A., Pandey, P.M., Misra, A. (eds) Optimization of Production and Industrial Systems. CPIE 2023. Lecture Notes in Mechanical Engineering. Springer, Singapore. https://doi.org/10.1007/978-981-99-8343-8_17.

[2] Deepti Raj, G., Prabadevi, B., Gopal, R. (2024). Evolution of Industry 4.0 and Its Fundamental Characteristics. In: Kumar, A., Sagar, S., Thangamuthu, P., Balamurugan, B. (eds) Digital Transformation. Disruptive Technologies and Digital Transformations for Society 5.0. Springer, Singapore. https://doi.org/10.1007/978-981-99-8118-2_1.

[3] Algabroun, Hatem, Muhammad Usman Iftikhar, Basim Al-Najjar and Danny Weyns. “Maintenance 4.0 Framework Using Self-Adaptive Software Architecture.” (2017).

[4] Pater, Ingeborg de and Mihaela Mitici. “Predictive maintenance for multi-component systems of repairables with Remaining-Useful-Life prognostics and a limited stock of spare components.” Reliab. Eng. Syst. Saf. 214 (2021): 107761.

[5] Yang Y, Yang M, Shangguan S, Cao Y, Yue W, Cheng K, Jiang P. An Industrial Case Study on the Monitoring and Maintenance Service System for a Robot-Driven Polishing Service System under Industry 4.0 Contexts. Systems. 2023; 11(7):376. https://doi.org/10.3390/systems11070376.

[6] Samigulina, G., Samigulina, Z. (2023). Biologically Inspired Unified Artificial Immune System for Industrial Equipment Diagnostic. In: Nicosia, G., et al. Machine Learning, Optimization, and Data Science. LOD 2022. Lecture Notes in Computer Science, vol 13811. Springer, Cham. https://doi.org/10.1007/978-3-031-25891-6_7.

[7] Lee, Jay, Masoud Ghaffari and S. Elmeligy. “Self-maintenance and engineering immune systems: Towards smarter machines and manufacturing systems.” Annu. Rev. Control. 35 (2011): 111-122.

[8] F. Rammig, K. Stahl and G. Vaz, "A framework for enhancing dependability in self-x systems by Artificial Immune Systems," 16th IEEE International Symposium on Object/component/service-oriented Real-time distributed Computing (ISORC 2013), Paderborn, Germany, 2013, pp. 1-10, doi: 10.1109/ISORC.2013.6913240.

[9] Rezvanian A, Vahidipour SM, Saghiri AM. CaAIS: Cellular Automata-Based Artificial Immune System for Dynamic Environments. Algorithms. 2024; 17(1):18. https://doi.org/10.3390/a17010018.

[10] S. S. P. Olaya, M. Wollschlaeger and S. S. Perez Olaya, "Control as an Industrie 4.0 component: Network-adaptive applications for control," 2017 22nd IEEE International Conference on Emerging Technologies and Factory Automation (ETFA), Limassol, Cyprus, 2017, pp. 1-4, doi: 10.1109/ETFA.2017.8247772.

[11] Chen, Zhaohui & Chen, Xu & Ding, Xiaobing & Wei, Liu & Tang, Tao & Zhou, Yu & Yu, Weiguo. (2024). Electromagnetic interference compensation method of TMR current sensor. Journal of Physics: Conference Series. 2703. 012060. 10.1088/1742-6596/2703/1/012060.

[12] “Achieving Highest System Angle Sensing Accuracy — Texas Instruments documentation.” https://www.ti.com.cn/cn/lit/an/sbaa539/sbaa539.pdf. Accessed: 09-04-2024.

[13] N. K. Bhaskarrao, C. S. Anoop and P. Kumar Dutta, "A linearizing interface circuit with phase-error compensated direct-digital output for TMR-based angular position sensor," 2017 IEEE International Instrumentation and Measurement Technology Conference (I2MTC), Turin, Italy, 2017, pp. 1-6, doi: 10.1109/I2MTC.2017.7969938.

[14] A. Zambrano and H. G. Kerkhoff, "Online digital offset voltage compensation method for AMR sensors," 2015 IEEE International Instrumentation and Measurement Technology Conference (I2MTC) Proceedings, Pisa, Italy, 2015, pp. 1512-1515, doi: 10.1109/I2MTC.2015.7151502.

[15] Alraho, S., Zaman, Q. & König, A. (2021). Wide Programmable Range Fourth-Order, Fully-Differential Sallen-Key MOSFET-C LPF for Impedance Spectroscopy Measurements and Self-X Sensory Electronics in Industry 4.0. tm - Technisches Messen, 88(s1), s77-s82.

[16] Zaman Q, Alraho S, König A. Low-Cost Indirect Measurements for Power-Efficient In-Field Optimization of Configurable Analog Front-Ends with Self-X Properties: A Hardware Implementation. Chips. 2023; 2(2):102-129.

[17] Gerken, Elena & König, A. (2023). A4.3 - Concept of a Self-X Sensory System and its first implementation on an XMR-based Angular Decoder Demonstrator. 57-58. 10.5162/SMSI2023/A4.3.

[18] Kocon M, Malesa M, Rapcewicz J. Ultra-Lightweight Fast Anomaly Detectors for Industrial Applications. Sensors. 2024; 24(1):161. https://doi.org/10.3390/s24010161.

[19] Gerken, Elena, Qummar Zaman, Senan Alraho and Andreas König. “Development of a Self-X Sensory Electronics for Anomaly Detection and its

Conceptual Implementation on an XMR-based Angular Decoder Prototype.” tm - Technisches Messen 90 (2023): 20 - 26.

[20] Alraho S, Zaman Q, Abd H, König A. Integrated Sensor Electronic Front-Ends with Self-X Capabilities. Chips. 2022; 1(2):83-120.

[21] A. Mohamed, M. Schmid, A. Tanwear, H. Heidari and J. Anders, "A Low Noise CMOS Sensor Frontend for a TMR-based Biosensing Platform," 2020 IEEE SENSORS, Rotterdam, Netherlands, 2020, pp. 1-4, doi: 10.1109/SENSORS47125.2020.9278826.

[22] S. Sarkar, "Novel Strategies for DAC based Offset Elimination Technique in Resistive Bridge Sensor," TENCON 2022 - 2022 IEEE Region 10 Conference (TENCON), Hong Kong, Hong Kong, 2022, pp. 1-6, doi: 10.1109/TENCON55691.2022.9977718.

[23] Vidal EG, Muñoz DR, Arias SIR, Moreno JS, Cardoso S, Ferreira R, Freitas P. Electronic Energy Meter Based on a Tunnel Magnetoresistive Effect (TMR) Current Sensor. Materials. 2017; 10(10):1134. https://doi.org/10.3390/ma10101134.